

Probing the Porosity of Cocrystallized MCM-49/ZSM-35 Zeolites by Hyperpolarized ^{129}Xe NMR

Yong Liu, Weiping Zhang,* Sujuan Xie, Longya Xu, Xiuwen Han, and Xinhe Bao*

State Key Laboratory of Catalysis, Dalian Institute of Chemical Physics, Chinese Academy of Sciences, 457 Zhongshan Road, Dalian 116023, China

Received: September 14, 2007; In Final Form: November 19, 2007

One- and two-dimensional ^{129}Xe NMR spectroscopy has been employed to study the porosity of cocrystallized MCM-49/ZSM-35 zeolites under the continuous flow of hyperpolarized xenon gas. It is found by variable-temperature experiments that Xe atoms can be adsorbed in different domains of MCM-49/ZSM-35 cocrystallized zeolites and the mechanically mixed counterparts. The exchange of Xe atoms in different types of pores is very fast at ambient temperatures. Even at very low temperature two-dimensional exchange spectra (EXSY) show that Xe atoms still undergo much faster exchange between MCM-49 and ZSM-35 analogues in the cocrystallized zeolites than in the mechanical mixture. This demonstrates that the MCM-49 and ZSM-35 analogues in cocrystallized zeolites may be stacked much closer than in the physical mixture, and some parts of intergrowth may be formed due to the partially similar basic structure of MCM-49 and ZSM-35.

1. Introduction

Generally, zeolites with single structure are directly applied in the field of chemical industry as catalysts, supports, adsorbents, ion exchangers, etc. However, the pure zeolite phase can be obtained only when the synthesis parameters are well controlled. Normally, the variations in the zeolite synthesis conditions will lead to the formation of cocrystallized zeolites with different phases. They may be regarded as the physical mixture in many cases; thus, their structure and properties are ignored. Only a few examples of intergrowth zeolites from cocrystallization, such as the intergrowths of zeolites X/A,¹ MFI/MEL,² FAU/EMT,³ and STF/SFF⁴ with the analogous basic structures, have been reported so far. In some cases composite materials are preferred for the combination of different structures and better performance in the catalytic reactions.^{5,6} Imbert et al.⁷ observed that the isomerization and hydrogen-transfer reactions could be inhibited within the pore systems of ZSM-5/ZSM-11 intergrowth zeolites for the *n*-decane cracking. Xu et al.⁸ reported MCM-22/ZSM-35 cocrystallized zeolites, which had a notable synergistic effect on the aromatization for butylene conversion and fluid catalytic cracking (FCC) gasoline updating. However, the most important characters—the framework structure and porosity—of these composite zeolites have not been well studied so far. Especially the porous structures of zeolites are very crucial for their shape selectivity in catalytic reactions. Although the high-resolution transmission electron microscopy provides the direct method for charactering the fine structures, there are disadvantages for study of the electron-beam-sensitive zeolites.⁹ More than one type of zeolite in the composites makes the porosity more complicated.

^{129}Xe NMR spectroscopy is a powerful tool for probing the porosity and species distribution in porous materials.^{10–13} However, the application of thermally polarized ^{129}Xe NMR to materials has been hampered by the relatively low sensitivity and long relaxation times (this is particularly the case for

amorphous materials like mesoporous silica¹⁴). The use of optical pumping techniques for the production of hyperpolarized (HP) xenon can increase sensitivity of several orders of magnitude ($\times 10^4$).^{15–17} This technique works at very low concentrations of xenon ($\sim 1\%$) under continuous flow, the contribution of Xe–Xe interactions is rather insignificant at ambient temperature, and the observed ^{129}Xe chemical shift could reflect mainly interactions between xenon atoms and the surface, i.e., the chemical composition of the surface and the geometry of the xenon environment in that particular site. These have made it very attractive for materials analysis.^{18–20}

In the present work, the continuous-flow hyperpolarized ^{129}Xe NMR has been employed to study the porous structure of MCM-49/ZSM-35 cocrystallized zeolites by variable-temperature experiments. For comparison, the porosities of pure-phased MCM-49 and ZSM-35 zeolite and their mechanical mixture are also investigated. Two-dimensional (2D) exchange NMR experiments are used to illustrate the exchange process of xenon in cocrystallized zeolites and their physical mixture counterparts in order to reveal their porous structure differences.

2. Experimental Section

2.1. Sample Preparation and Characterization. MCM-49, ZSM-35, and MCM-49/ZSM-35 cocrystallized zeolites were synthesized as follows. Typically, the molar composition of the gel is 4.0–7.5CHA:4.0–2.6HMI:3.0Na₂O:30SiO₂:Al₂O₃:750–900H₂O, where CHA and HMI are cyclohexylamine and hexamethylenimine, respectively. After aging, the gel was transferred into the stainless steel autoclave, where the crystallization was performed dynamically at given temperatures for a few days. After crystallization all samples were thoroughly washed with deionized water and dried at 393 K. After calcination to remove the template, the Na-type samples were ion-exchanged with an aqueous NH₄NO₃ solution to get the NH₄ type and then calcined again at 793 K for 2 h in air to get the H-type zeolites. Before ^{129}Xe NMR measurements the samples were pressed, crushed, and sieved into 20–40 mesh particles. The crystalline phases of these samples have been confirmed

* To whom correspondence should be addressed: Ph +86-411-8437 9976; Fax +86-411-8469 4447; e-mail wpzhang@dicp.ac.cn, xhbao@dicp.ac.cn.

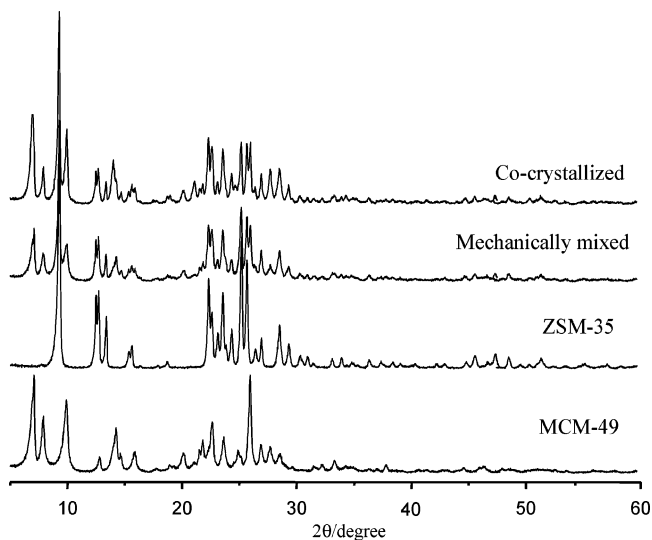


Figure 1. XRD patterns of calcined MCM-49, ZSM-35, mechanically mixed, and cocrystallized zeolites.

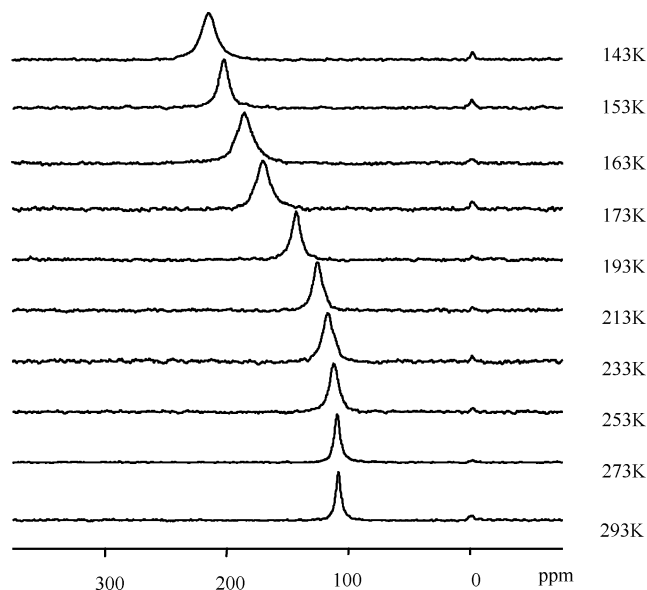


Figure 2. Temperature-dependent hyperpolarized ^{129}Xe NMR spectra of Xe adsorbed in pure-phased MCM-49 zeolite. The temperature is varied from 293 to 143 K.

by XRD patterns which were obtained at room temperature on a Rigaku D/max-rb diffractometer with Cu $K\alpha$ radiation. The resultant zeolite with the MWW structure is MCM-49 instead of MCM-22 although they can be hardly distinguished after calcinations (see Figure S1 in the Supporting Information).²¹ The weight content of MCM-49 and ZSM-35 in the cocrystallized zeolites is about 45% and 55%, respectively, which could be estimated from XRD patterns by the internal standard method using fluorite as the reference. The weight ratio of mechanically mixed sample was the same as that in the cocrystallized zeolites. The BET surface area and pore volume were measured at 77 K on a Quantachrome NOVA Automated system. The measurement error of surface area and pore volume was estimated to less than 10%.

2.2. Continuous-Flow Hyperpolarized ^{129}Xe NMR. ^{129}Xe NMR experiments were carried out at 110.6 MHz on the Varian Infinity-plus 400 spectrometer using a 7.5 mm probe. Prior to each experiment, samples were subjected to dehydration at 723 K under vacuum ($<10^{-5}$ Torr) for ca. 20 h. Optical polarization of xenon was achieved with an apparatus similar to that in ref

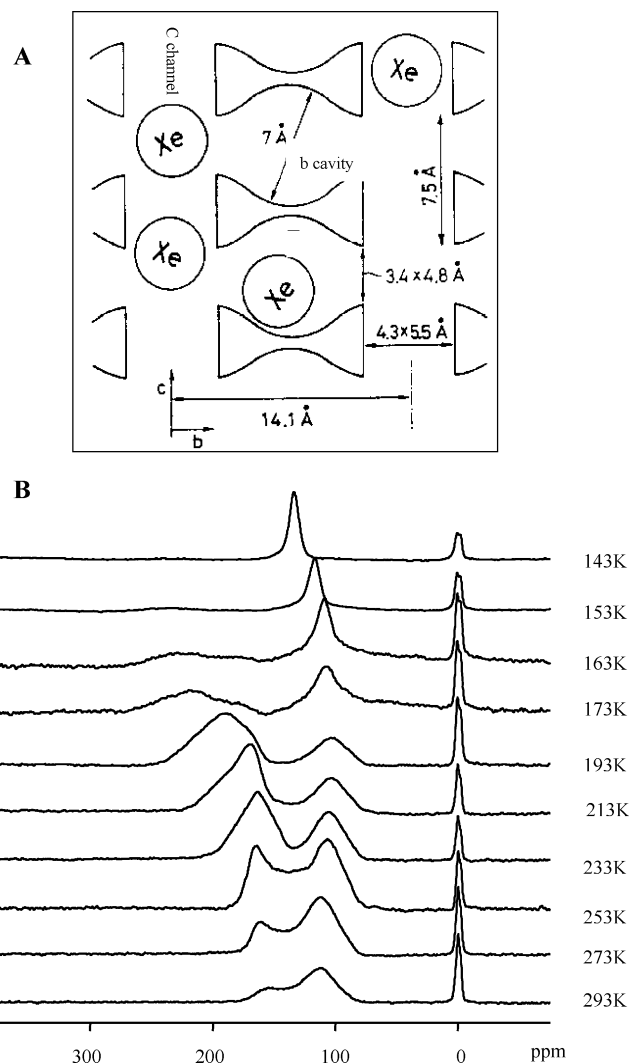


Figure 3. (A) Schematic structure of ZSM-35 zeolite (from ref 23 with permission). (B) Temperature-dependent hyperpolarized ^{129}Xe NMR spectra of Xe adsorbed in pure-phased ZSM-35 zeolite. The temperature is varied from 293 to 143 K.

TABLE 1: N_2 Adsorption Results of MCM-49, ZSM-35, Mechanically Mixed, and Cocrystallized Zeolites

	MCM-49	ZSM-35	mechanically mixed	cocrystallized
BET surface area (m^2/g)	497	310	375	423
micropore vol (cm^3/g)	0.17	0.11	0.14	0.16

19, with the optical pumping cell in the fringe field of the spectrometer magnet and 60 W diode laser array (Coherent FAP-System). A flow of 1% Xe–1% N_2 –98% He gas mixture was delivered at the rate of 200–250 cm^3/min to the sample in detection region via plastic tubing. Variable-temperature NMR measurements were also performed in the range 143–298 K. All one-dimensional spectra were acquired with 3.0 μs $\pi/2$ pulse, 100–200 scans, and 2 s recycle delay. The chemical shifts were referenced to the signal of xenon gas. Although this line was temperature dependent, its chemical shift variation would not be more than 1 ppm in the whole range of measurements because of the very low concentration of xenon. The two-dimensional exchange experiments (2D-EXSY) were performed at 143 K using a $90^\circ-t_1-90^\circ-\tau_m-90^\circ-t_2$ pulse sequence in TPPI mode. Each 2D spectrum was acquired with 32 points in the t_1 dimension and 1024 points in the t_2 dimension. Before

Fourier transformation the t_1 dimension was zero-filled to 256 points. Mixing times were varied from 0.1 to 20 ms.

3. Results and Discussion

3.1. XRD and Nitrogen Adsorption. XRD patterns of calcined zeolites MCM-49, ZSM-35, mechanically mixed, and cocrystallized zeolites are shown in Figure 1. MCM-49 and ZSM-35 zeolite with typical characters of MWW and FER have high crystallinity. MCM-49/ZSM-35 cocrystallized zeolites and the mechanically mixed sample show similar diffractions in XRD patterns. The results from the BET surface area and pore volume (see Table 1) show no big difference between cocrystallized zeolites and mechanical mixture. So it cannot get any valuable information from the routine XRD and nitrogen adsorption.

3.2. HP ^{129}Xe NMR of Pure-Phased MCM-49 and ZSM-35 Zeolite. MCM-49 zeolite with the MWW structure consists of two types of noninterconnected pores: the sinusoidal channels with 10-MR openings (0.41×0.51 nm) and the supercages with 12-MR cross section (0.71 nm in diameter). The structure of MCM-49 is virtually identical with that of MCM-22 in the calcined form.²¹ Figure 2 shows the variable-temperature hyperpolarized ^{129}Xe NMR spectra of Xe adsorbed in pure-phased MCM-49. The peaks at 0 ppm in the spectra are from xenon in the gas phase. All signals at lower field are originated from the adsorbed xenon in the zeolites. The chemical shifts of the line from Xe in MCM-49 increase from 115 to 197 ppm when the temperature decreases from 293 to 143 K. This is a general trend in variable-temperature ^{129}Xe NMR experiments mainly due to the increase of the Xe–Xe interactions at lower temperatures even if the partial pressure of xenon is quite small. Just like the case in MCM-22, this line may be attributed to Xe adsorbed in the supercages of MCM-49 alone²² or the superposition of the two signals from Xe adsorbed in supercages and 10-MR channels.^{20c} As pointed out by Gédéon et al.,²³ the similarity of the mean free paths of Xe in these two types of pores may result in only a single line in the ^{129}Xe NMR spectrum. In our case Xe atoms adsorbed in the supercages and 10-MR channels of MCM-49 may also undergo fast exchange even at the very low temperatures, and the two resonances coalesce to produce a single line.

The porous structure of ZSM-35 consists of a bidimensional channel network: cylindrical c channels (10-MR elliptical cross section, 0.42×0.54 nm) and b channels parallel to the c and b axes, respectively. In the b -direction, channels are approximately spherical cavities with a diameter of about 0.7 nm and with two opposite windows (8-MR, 0.35×0.48 nm) opening onto the c channels (see Figure 3A). At room temperature, the hyperpolarized ^{129}Xe NMR spectra of Xe adsorbed in pure-phased ZSM-35 show two lines at 155 and 110 ppm (see Figure 3B), which may correspond to Xe adsorbed in the two types of voids, i.e., channels and cavities, respectively.^{23,24} The line at 155 ppm shifts to the downfield when the temperature decreases. On the contrary, the chemical shift of the high field line at 110 ppm is almost independent of the temperature between 293 and 163 K. This may be due to the b cavities can accommodate only one xenon atom. While in the channel c , Xe atoms can be packed so that Xe–Xe interactions become stronger with decreasing of the temperature, which leads to downfield shift of the line from Xe in the channels. There is a very obvious change in the shape of the signal from Xe in the channels (Figure 3B), which is probably due to the chemical shift anisotropy.^{20c} The relative intensities of these two lines also change with the temperature. At room temperature the

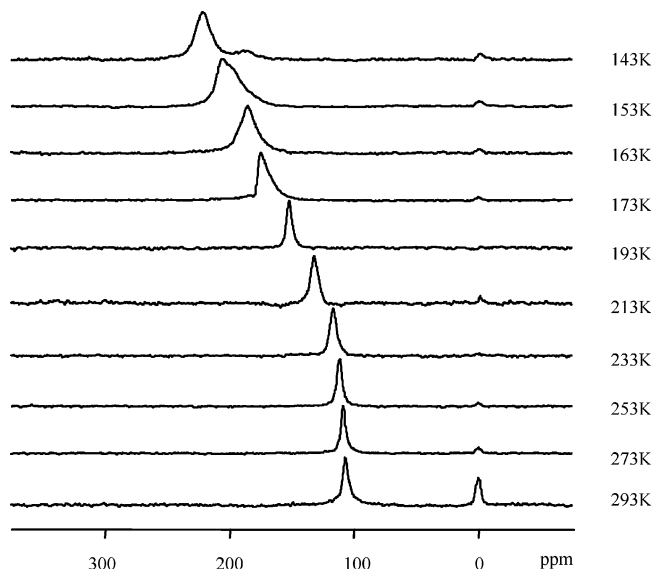


Figure 4. Temperature-dependent hyperpolarized ^{129}Xe NMR spectra of Xe adsorbed in MCM-49/ZSM-35 cocrystallized zeolites. The temperature is varied from 293 to 143 K.

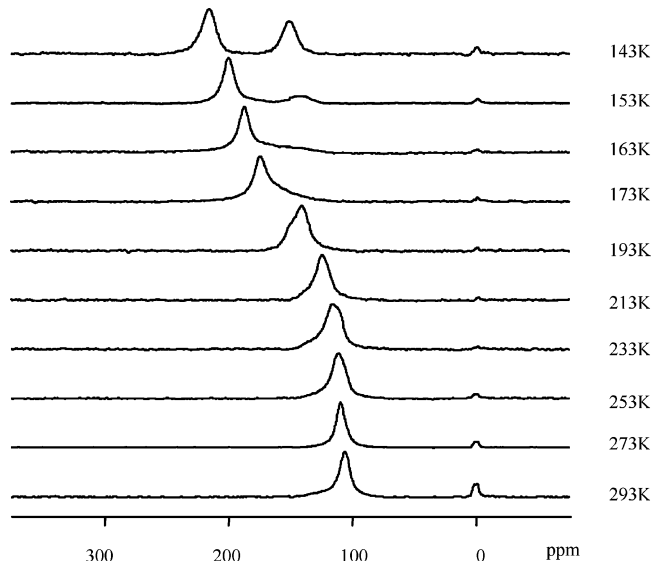


Figure 5. Temperature-dependent hyperpolarized ^{129}Xe NMR spectra of Xe adsorbed in MCM-49/ZSM-35 mechanically mixed zeolites. The temperature is varied from 293 to 143 K.

intensity of the line in high field is stronger, so Xe atoms may prefer to stay in the cavities. At lower temperatures no more Xe atoms could enter the cavities due to the slower mobility of Xe atoms, so Xe atoms would prefer to stay in the channels, and the intensity of the line in low field grows up. This is consistent with what Springuel-Huet et al. found in the variable-temperature and -pressure ^{129}Xe NMR experiments.^{20c,23,24} Below 173 K the intensity of the line in low field weakens and vanishes at 143 K. This is probably due to more xenon condensation in the channels and longer residence time of xenon in the adsorbed state with decreasing the temperature, which may lead to the significant decrease of the exchange with the gas phase and the subsequent polarization of Xe in the channels. The high level of polarization cannot be maintained due to the fast relaxation rate of Xe.^{20d} The signal saturation by the pulses may exist but its contribution may be limited at 143 K because the signal intensity was nearly unchanged when increasing the pulse delay up to 60 s, and the signals observed were from the

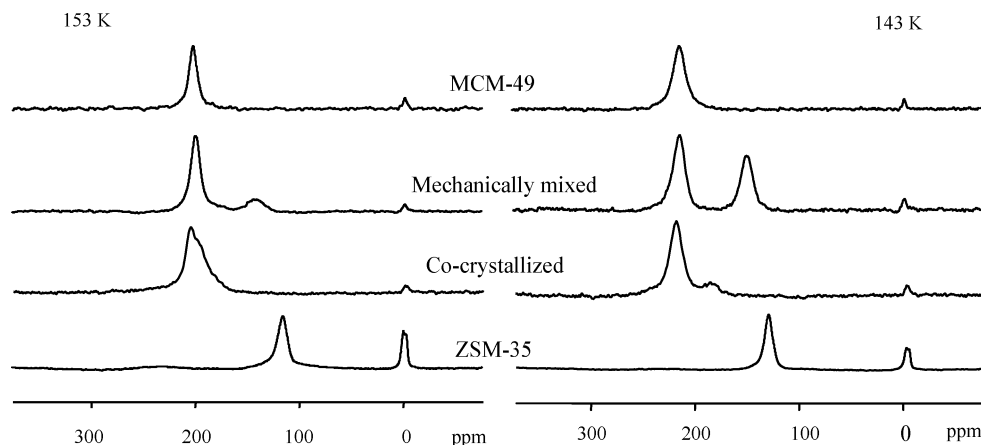


Figure 6. Hyperpolarized ^{129}Xe NMR spectra of Xe adsorbed in MCM-49, mechanically mixed, cocrystallized, and ZSM-35 zeolites at 153 and 143 K.

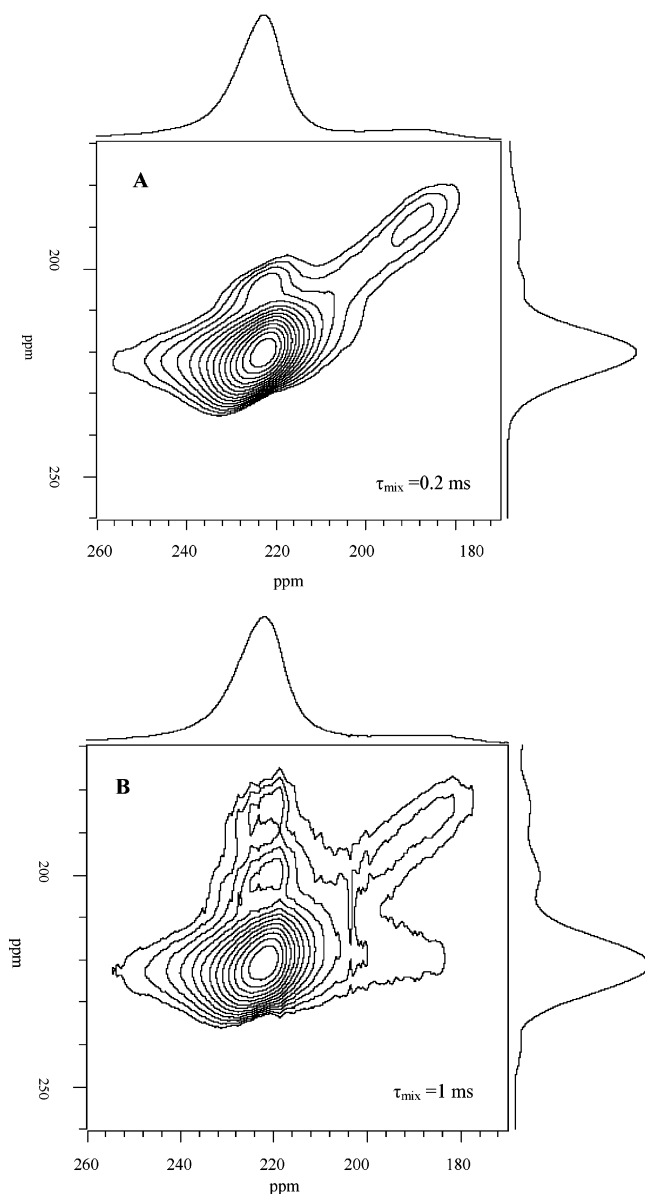


Figure 7. Hyperpolarized ^{129}Xe 2D-EXSY NMR spectra of cocrystallized zeolites at 143 K with different mixing time: (A) $\tau_{\text{mix}} = 0.2$ ms; (B) $\tau_{\text{mix}} = 1$ ms.

hyperpolarized xenon not from the thermally polarized xenon since almost no signal appeared when switching the laser power off (see Figures S2 and S3 in the Supporting Information).

3.3. HP ^{129}Xe NMR of Cocrystallized MCM-49/ZSM-35 Zeolites and Mechanically Mixed Counterparts.

The cocrystallized zeolites have the weight ratio of 45% MCM-49 and 55% ZSM-35 from XRD measurements. Figure 4 shows their hyperpolarized ^{129}Xe NMR spectra. There is only one signal in the low field above 193 K. When the temperature decreases to 173 K and lower, it becomes asymmetric and a new signal appears in the high field at 143 K. This means there are at least two types of pores in the MCM-49/ZSM-35 cocrystallized zeolites, and the faster exchange of Xe atoms between these two types of pores exists above 173 K. In order to get a better understanding of the porous structure in cocrystallized zeolites, we prepared a mechanical mixture with the same weight composition as the cocrystallized zeolites. Figure 5 shows the VT hyperpolarized ^{129}Xe NMR spectra. At room temperature, there is nearly a single line, which may be assigned to the overlap signals of Xe in MCM-49 and cavities of ZSM-35. The Xe signal in ZSM-35 is not so clear probably due to the much smaller surface area of ZSM-35 compared to MCM-49. However, when the temperature decreases below 233 K, an asymmetric signal appears gradually in the low field, and a new peak becomes much more obvious in the high field at 143 K compared to the cocrystallized zeolites. This also indicates that there are at least two types of pores in the mechanical mixture. For a better assignment of these two signals, Figure 6 shows the HP ^{129}Xe NMR spectra of the four samples with xenon adsorption at 153 and 143 K. From above discussion we know that the exchange of Xe atoms in different pores of the individual zeolite is quite slow at such low temperatures, so the single signal in the ^{129}Xe NMR spectrum of MCM-49 and ZSM-35 may represent the characteristic structure of zeolite MCM-49 and ZSM-35, respectively. It can be seen from Figure 6 that the low-field signal in the cocrystallized and mechanically mixed zeolites should come from the Xe adsorbed in MCM-49 analogues, while the high-field one should be assigned to Xe adsorbed in ZSM-35 analogues. Xe adsorbed in these two domains may still undergo exchange because the signal from Xe adsorbed in ZSM-35 analogues shifts to the lower field in cocrystallized and mechanically mixed zeolites compared to that in the pure-phased ZSM-35 zeolite. At 143 K the chemical shift difference ($\Delta\delta$) of xenon in these two domains is 34 ppm for the cocrystallized zeolites, which is less than that of 65 ppm for the mechanically mixed ones. This means that the Xe exchange is much faster between MCM-49 and ZSM-35 analogues in the cocrystallized zeolites than in the mechanically mixed counterparts, which may also demonstrate that the stacking of these two analogues is different in cocrystallized

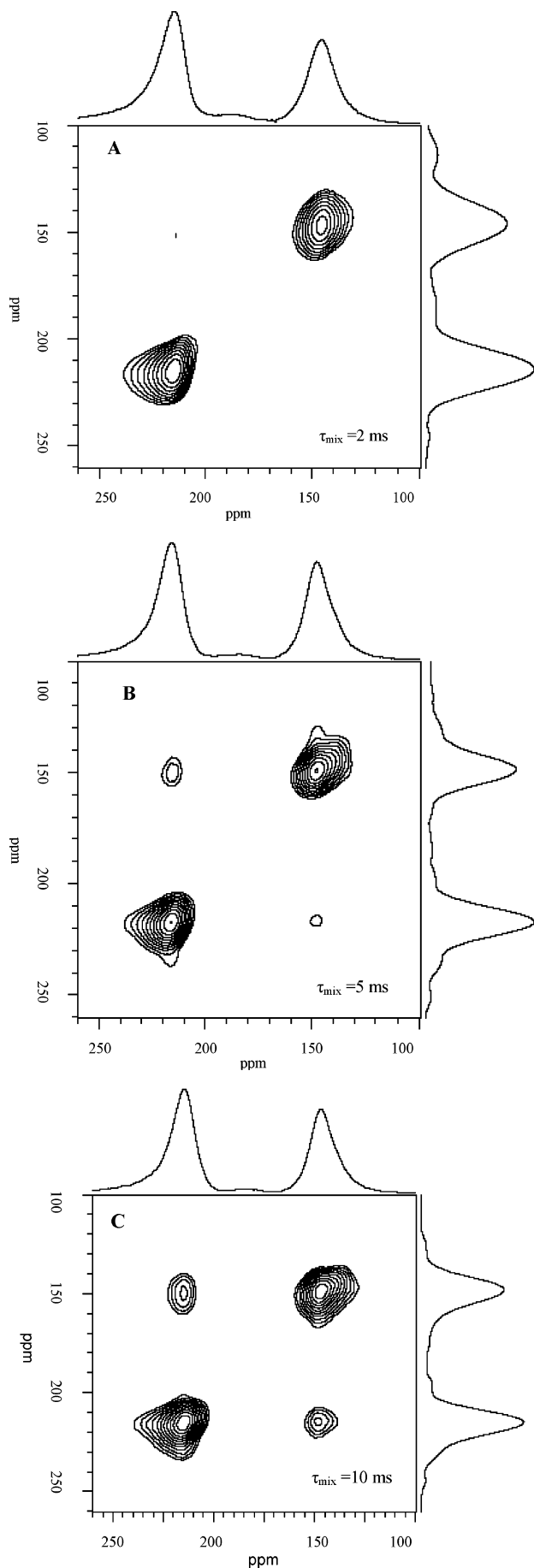


Figure 8. Hyperpolarized ^{129}Xe 2D-EXSY NMR spectra of mechanically mixed zeolites at 143 K with different mixing time: (A) $\tau_{\text{mix}} = 2$ ms; (B) $\tau_{\text{mix}} = 5$ ms; (C) $\tau_{\text{mix}} = 10$ ms.

and mechanically mixed zeolites. Similar phenomena have also been found by Liu et al. in the characterization of microporous/mesoporous composite materials by HP ^{129}Xe NMR.²⁵ The exchange rate of Xe atoms between Al-MCM-41 (or Al-SBA-15) and ZSM-5 is lower in the mechanical mixture than in the corresponding composite materials.

3.4. HP ^{129}Xe Two-Dimensional Exchange Spectra. A powerful tool for the study of exchange process is 2D-exchange NMR spectroscopy (EXSY) as introduced by Jeener et al.,²⁶ and this technique can be extended to study the dynamic processes of adsorbed Xe in porous solid materials.²⁷ 2D EXSY is achieved by monitoring frequencies before and after a so-called mixing time, τ_{mix} , during which spin exchange and/or molecular reorientation motions can occur. Changes in the NMR frequencies manifest themselves as off-diagonal intensities in a 2D exchange spectrum, which depends on the mixing time. The 2D spectrum represents a direct mapping of the joint probability density of finding a Xe atom in a given adsorption site (thus with a given NMR frequency) and, after τ_{mix} , finding the same Xe atom in another adsorption site (with another NMR frequency). The cross-peaks indicate an exchange of xenon atoms between the corresponding environments on the diagonal within the period of τ_{mix} .²⁸ To see more clearly the exchange of adsorbed Xe between two different domains and how fast these exchange processes might be, HP ^{129}Xe 2D EXSY spectra were recorded at 143 K for cocrystallized and mechanically mixed zeolites, which are shown in Figures 7 and 8, respectively. The corresponding 1D spectrum is displayed above the EXSY for clarity. The polarization of Xe mainly comes from the hyperpolarized Xe in the 2D experiments because nearly no signal appeared at 143 K when switching the laser power off (see Figure S4 in the Supporting Information). The absence of cross-peaks in Figure 7A demonstrates that the exchange between MCM-49 and ZSM-35 analogues in cocrystallized zeolites does not occur during short exchange times $\tau_{\text{mix}} \leq 0.2$ ms. The presence of marked cross-peaks between two ^{129}Xe NMR peaks assigned to xenon in MCM-49 and ZSM-35 analogues in Figure 7B suggests that the exchange of xenon between these environments exists at a time scale of 1 ms. So, for cocrystallized zeolites the Xe exchange takes place between MCM-49 and ZSM-35 domains in the time range 0.2–1 ms. For the mechanically mixed sample 2D exchange spectra show that there is no Xe exchange between MCM-49 and ZSM-35 zeolites at the τ_{mix} of 2 ms (Figure 8A). The xenon exchange emerges when τ_{mix} increases to 5 ms and becomes rapidly for the appearance of strong cross-peaks when τ_{mix} increases further to 10 ms (Figure 8B,C). So, for mechanically mixed zeolites the Xe exchange is similar to intercrystalline diffusion between these two zeolites, which occurs in the time range 2–5 ms. It is much slower than that in the cocrystallized zeolites. This reveals that the MCM-49 and ZSM-35 analogues in cocrystallized zeolites may stay much closer than in the physical mixture, and some intergrowth parts may be formed due to the partially similar basic structure of MCM-49 and ZSM-35.

4. Conclusions

The porous structures of cocrystallized MCM-49/ZSM-35 zeolites have been studied by the continuous-flow hyperpolarized ^{129}Xe NMR. Different adsorption domains of Xe in MCM-49/ZSM-35 cocrystallized zeolites and mechanically mixed counterparts can be directly detected by variable-temperature experiments. The exchange of Xe atoms in different pores is very fast at ambient temperatures. The 2D exchange NMR spectra (EXSY) show that Xe atoms still undergo much faster

exchange between MCM-49 and ZSM-35 analogues in the cocrystallized zeolites than in the mechanically mixed counterparts even at very low temperature. This demonstrates that the MCM-49 and ZSM-35 analogues in cocrystallized zeolites may be stacked much closer than in the physical mixture. Thus, some intergrowth parts may be formed in the crystals due to the partially similar basic structure of MCM-49 and ZSM-35.

Acknowledgment. We thank Professor S.-B. Liu (Academia Sinica, Taiwan) for helpful discussions with the ^{129}Xe optical pumping system. We are grateful for the financial support of the National Natural Science Foundation of China (Grants 20573106, 20403017) and the Ministry of Science and Technology of China through the National Key Project of Fundamental Research (Grants 2003CB615806, 2003CB615802). We also thank the anonymous reviewers for the fruitful discussion and suggestions.

Supporting Information Available: XRD patterns of MCM-49 and MCM-22 before and after calcination and the identification of hyperpolarized Xe signal saturation or not. This information is available free of charge via the Internet at <http://pubs.acs.org>.

References and Notes

- (1) de Vos Burchart, E.; Jansen, J. C.; van Bekkum, H. *Zeolites* **1989**, *9*, 432.
- (2) Millward, G. R.; Ramdas, S.; Thomas, J. M.; Barlow, M. T. *J. Chem. Soc., Faraday Trans. 2* **1983**, *79*, 1075.
- (3) (a) Li, H. X.; Armor, J. N. *Microporous Mater.* **1997**, *9*, 51. (b) Goossens, A. M.; Wouters, B. H.; Grobet, P. J.; Buschmann, V.; Fiermans, L.; Martens, J. A. *Eur. J. Inorg. Chem.* **2001**, 1167.
- (4) Villaescusa, L. A.; Zhou, W.; Morris, R. E.; Barrett, P. A. *J. Mater. Chem.* **2004**, *14*, 1982.
- (5) Zones, S. I.; Davis, M. E. *Curr. Opin. Solid State Mater. Chem.* **1996**, *1*, 107.
- (6) Smirniotis, P.G.; Davydov, L.; Ruchenstein, E. *Catal. Rev.—Sci. Eng.* **1999**, *41*, 43.
- (7) Francesconi, M. S.; Lopez, Z. E.; Uzcategui, D.; Gonzalez, G.; Hernandez, J. C.; Uzcategui, A.; Loaiza, A.; Imbert, F. E. *Catal. Today* **2005**, *107–108*, 809.
- (8) Niu, X. L.; Song, Y. Q.; Xie, S. J.; Liu, S. L.; Wang, Q. X.; Xu, L. Y. *Catal. Lett.* **2005**, *103*, 211.
- (9) Terasaki, O.; Ohsuna, T. *Catal. Today* **1995**, *23*, 201.
- (10) (a) Ito, T.; Fraissard, J. *J. Chem. Phys.* **1982**, *76*, 5225. (b) Ripmeester, J. A. *J. Am. Chem. Soc.* **1982**, *104*, 289.
- (11) Raftery, D.; Chmelka, B. F. *NMR* **1994**, *30*, 111.
- (12) Ratcliffe, C. I. *Annu. Rep. NMR Spectrosc.* **1998**, *36*, 123.
- (13) Bonardet, J. L.; Fraissard, J.; Gédéon, A.; Springuel-Huet, M. A. *Catal. Rev.—Sci. Eng.* **1999**, *41*, 115.
- (14) Pietrass, T.; Kneller, J. M.; Assink, R. A.; Anderson, M. T. *J. Phys. Chem. B* **1999**, *103*, 8837.
- (15) Happer, W.; Miron, E.; Schaefer, S.; Schreiber, D.; van Wingen, W. A.; Zeng, X. *Phys. Rev. A* **1984**, *29*, 3092.
- (16) (a) Raftery, D.; Long, H.; Meersmann, T.; Grandinetti, P. J.; Reven, L.; Pines, A. *Phys. Rev. Lett.* **1991**, *66*, 584. (b) Raftery, D.; MacNamara, E.; Fisher, G.; Rice, C. V.; Smith, J. *J. Am. Chem. Soc.* **1997**, *119*, 8746. (c) Brunner, E.; Seydoux, R.; Haake, M.; Pines, A.; Reimer, J. A. *J. Magn. Reson.* **1998**, *130*, 145.
- (17) (a) Pietrass, T.; Gaede, H. *Adv. Mater.* **1995**, *7*, 826. (b) Brunner, E. *Concepts Magn. Reson.* **1999**, *11*, 313.
- (18) (a) Haake, M.; Pines, A.; Reimer, J. A.; Seydoux, R. *J. Am. Chem. Soc.* **1997**, *119*, 11711. (b) Meersmann, T.; Logan, J. W.; Simonutti, R.; Caldarelli, S.; Comotti, A.; Sozzani, P.; Kaiser, L. G.; Pines, A. *J. Phys. Chem. A* **2000**, *104*, 11665. (c) Kneller, J. M.; Soto, R. J.; Surber, S. E.; Colomer, J. F.; Fonseca, A.; Nagy, J. B.; Van Tendeloo, G.; Pietrass, T. *J. Am. Chem. Soc.* **2000**, *122*, 10591.
- (19) (a) Moudrakovski, I. L.; Nossov, A.; Lang, S.; Breeze, S. R.; Ratcliffe, C. I.; Simard, B.; Santyr, G.; Ripmeester, J. A. *Chem. Mater.* **2000**, *12*, 1181. (b) Zhang, W. P.; Ratcliffe, C. I.; Moudrakovski, I. L.; Mou, C. Y.; Ripmeester, J. A. *Anal. Chem.* **2005**, *77*, 3379. (c) Huang, S. J.; Huang, C. H.; Chen, W. H.; Sun, X. P.; Zeng, X. Z.; Lee, H. K.; Ripmeester, J. A.; Mou, C. Y.; Liu, S. B. *J. Phys. Chem. B* **2005**, *109*, 681.
- (20) (a) Nossov, A.; Haddad, E.; Guenneau, F.; Mignon, C.; Gédéon, A.; Grosso, D.; Babonneau, F.; Bonhomme, C.; Sanchez, C. *Chem. Commun.* **2002**, 2476. (b) Nossov, A.; Guenneau, F.; Springuel-Huet, M. A.; Haddad, E.; Montouillout, V.; Knott, B.; Engelke, F.; Fernandez, C.; Gédéon, A. *Phys. Chem. Chem. Phys.* **2003**, *5*, 4479. (c) Springuel-Huet, M. A.; Guenneau, F.; Gédéon, A.; Corma, A. *J. Phys. Chem. C* **2007**, *111*, 5694. (d) Nader, M. H.; Guenneau, F.; Salame, P.; Launay, F.; Semmer, V.; Gédéon, A. *J. Phys. Chem. C* **2007**, *111*, 13564.
- (21) Lawton, S. L.; Fung, A. S.; Kennedy, G. J.; Alemany, L. B.; Chang, C. D.; Hatzikos, G. H.; Lissy, D. N.; Rubin, M. K.; Timken, H. C.; Steuernagel, S.; Woessner, D. E. *J. Phys. Chem.* **1996**, *100*, 3788.
- (22) Chen, F.; Deng, F.; Chen, M. J.; Yue, Y.; Ye, C. H.; Bao, X. H. *J. Phys. Chem. B* **2001**, *105*, 9426.
- (23) Springuel-Huet, M. A.; Nossov, A.; Guenneau, F.; Fornes, V.; Corma, A.; Fraissard, J.; Gédéon, A. *Stud. Surf. Sci. Catal.* **2004**, *154*, 1204.
- (24) Ito, T.; Springuel-Huet, M. A.; Fraissard, J. *Zeolites* **1989**, *9*, 68.
- (25) Sakthivel, A.; Huang, S. J.; Chen, W. H.; Lan, Z. H.; Chen, K. H.; Kim, T. W.; Ryoo, R.; Chiang, A. S. T.; Liu, S. B. *Chem. Mater.* **2004**, *16*, 3168.
- (26) Jeener, J.; Meier, B. H.; Bachmann, P.; Ernst, R. R. *J. Chem. Phys.* **1979**, *71*, 4546.
- (27) (a) Sears, D. N.; Demko, B. A.; Ooms, K. J.; Wasylshen, R. E.; Huang, Y. *Chem. Mater.* **2005**, *17*, 5481. (b) Knagge, K.; Smith, J. R.; Smith, L. J.; Buriak, J.; Raftery, D. *Solid State Nucl. Magn. Reson.* **2006**, *29*, 85.
- (28) (a) Larsen, R. G.; Shore, J.; Schmidt-Rohr, K.; Emsley, L.; Pines, A.; Janicke, M.; Chmelka, B. F. *Chem. Phys. Lett.* **1993**, *214*, 220. (b) Moudrakovski, I. L.; Ratcliffe, C. I.; Ripmeester, J. A. *Appl. Magn. Reson.* **1995**, *8*, 385.